No Evidence for Critical Balance in Field-aligned Alfvénic Solar Wind Turbulence

Daniele Telloni[1] , Francesco Carbone[2] , Roberto Bruno[3] , Luca Sorriso-Valvo[4,5] , Gary P. Zank[6,7] ,
Laxman Adhikari[6] , and Peter Hunana[8,9]

[1] National Institute for Astrophysics—Astrophysical Observatory of Torino Via Osservatorio 20, I-10025 Pino Torinese, Italy; daniele.telloni@inaf.it
[2] National Research Council—Institute of Atmospheric Pollution Research c/o University of Calabria, I-87036 Rende, Italy
[3] National Institute for Astrophysics—Institute for Space Astrophysics and Planetology Via del Fosso del Cavaliere 100, I-00133 Roma, Italy
[4] Escuela Politécnica Nacional, Departamento de Física Ladron de Guevera E11-253, Quito 170517, Ecuador
[5] National Research Council—Institute for Science and Technology of Plasmas Via Amendola 122/D, I-70126 Bari, Italy
[6] University of Alabama, Center for Space Plasma and Aeronomic Research Huntsville, AL 35805, USA
[7] University of Alabama, Department of Space Science Huntsville, AL 35805, USA
[8] Instituto de Astrofísica de Canarias La Laguna, Tenerife, E-38205, Spain
[9] Universidad de La Laguna La Laguna, Tenerife, E-38206, Spain

Abstract

The properties of Alfvénic solar wind turbulence have been studied for decades using spacecraft measurements. In particular, the observation of spectral anisotropy of magnetic fluctuations has stimulated the development of several phenomenological models, one of the most popular being critical balance. However, the experimental validation of these models is intrinsically difficult because of the one-dimensional nature of the measurements provided by spacecraft instrumentation. In this work, a thorough search is performed in the *Wind* spacecraft database to extract samples of field-aligned fast solar wind, which allow the precise estimation of the parallel spectral properties of the magnetic fluctuations, and of their intermittency. Hilbert spectral analysis is used, in order to eliminate the possible role of nonstationarity and large-scale structures. Our results indicate that the spectral anisotropy predicted by the critical balance theory is not observed in the selected database, thus questioning the validity of the critical balance in the solar wind turbulence. A stochastic process characterized by a $-5/3$ spectral scaling, which is not necessarily attributed to usual turbulence, as indicated by the absence of intermittency, is indeed observed in the analyzed data samples.

Unified Astronomy Thesaurus concepts: Interplanetary turbulence (830); Solar wind (1534); Space plasmas (1544); Alfven waves (23); Interplanetary medium (825); Magnetohydrodynamics (1964)

1. Introduction

The presence of a local magnetic field in a space plasma causes the breaking of isotropic symmetry in the turbulence properties. This is true of the solar wind, which is de facto a unique laboratory for studying turbulence in space plasmas (Bruno & Carbone 2013). Anisotropy in solar wind turbulence develops in different ways (Horbury et al. 2012), which are, however, all strictly but not trivially related to each other (all of them descend from the preferential energy transfer perpendicular to the mean magnetic field, as predicted by several theories of plasma turbulence; Shebalin et al. 1983; Goldreich & Sridhar 1995; Boldyrev 2006; Zank et al. 2017): (i) elongation of eddies in the mean magnetic field direction (wavevector anisotropy, $k_\perp > k_\parallel$), (ii) different power levels at a particular wavenumber relative to the magnetic field direction (power anisotropy, $P(k_\perp) \neq P(k_\parallel)$; e.g., Adhikari et al. 2017), and (iii) different turbulent power scaling in different directions relative to the magnetic field (spectral index anisotropy, $\alpha_\perp \neq \alpha_\parallel$).

Phenomenological models of Alfvénic turbulence lead to anisotropy in wavevector space. In these models, the crucial parameter regulating the strength of turbulence is the ratio χ between the linear Alfvén timescale $\tau_A \simeq \ell_\parallel / \upsilon_A$ representing the typical propagation time of an Alfvén wave along an eddy of size $\ell_\parallel$ (where υ_A is the Alfvén speed) and the nonlinear decay timescale $\tau_{nl} \simeq \ell_\perp / \delta u(\ell_\perp)$ representing the perpendicular eddy turnover time (where $\delta u(\ell_\perp)$ is the fluctuation velocity across an eddy of size $\ell_\perp$):

$$\chi = \frac{\tau_A}{\tau_{nl}} \simeq \frac{\ell_\parallel \delta u}{\ell_\perp \upsilon_A}. \qquad (1)$$

If $\chi \ll 1$, oppositely propagating Alfvén wave packets experience many interactions before their energy is transferred to smaller scales (Iroshnikov 1964; Kraichnan 1965). Since χ is small when the amplitude of the fluctuations is small, this condition is found in cases of weak turbulence. Conversely, for $\chi \gg 1$ the Alfvénic fluctuations undergo multiple decays before their interaction. Note that both these initial conditions naturally evolve toward a state where the nonlinear and Alfvén timescales become comparable (i.e., the nonlinear cascade occurs within a single interaction; Montgomery & Turner 1981; Shebalin et al. 1983): equating the two timescales ($\chi \simeq 1$) leads to a scaling of $k_\parallel \propto k_\perp^{2/3}$. If the turbulence remains in this "critically balanced" state (strong turbulence; Goldreich & Sridhar 1995), this implies wavevector anisotropy of $k_\perp \gg k_\parallel$ at small scales and an anisotropic energy cascade, which results in the anisotropy of the spectral index. The turbulent energy scales differently in parallel and perpendicularly components (with respect to the local mean magnetic field) as $E(k_\perp) \propto k_\perp^{-5/3}$ and $E(k_\parallel) \propto k_\parallel^{-2}$.

Note that the Goldreich & Sridhar (1995) theory applies only to turbulence driven by nonlinear interactions among oppositely directed Alfvén modes carrying equal energies, E^+ and E^-—that is, only to turbulence with vanishing cross-helicity ($\sigma_c = (E^+ - E^-)/(E^+ + E^-) \simeq 0$), a condition usually not

found in the imbalanced fast solar wind, characterized by uni-directional outwardly oriented Alfvén wave propagation ($\sigma_c \simeq \pm 1$)). However, the critical balance conjecture has been more recently extended also to imbalanced cascades, with $\sigma_c \simeq 1$, by Lithwick et al. (2007). It turns out that in addition to imbalanced turbulence, the energy spectra perpendicular and parallel to the local mean magnetic field are predicted to scale like $k_\perp^{-5/3}$ and $k_\parallel^{-2}$, respectively.

The measurement of the spectral index anisotropy at fluid scales thus represents a crucial diagnostic in providing observational evidence for critical balance in the solar wind and for distinguishing the physical processes taking place. Interplanetary observations can be used hence to glean information about the wavevector anisotropy of solar wind turbulence, by measuring the power spectrum in the direction parallel to the local mean magnetic field.

Despite the considerable restrictions of such a measurement imposed by single point observations, noticeable advances have been made recently in studying the turbulence anisotropy, through novel methods and multi-spacecraft data techniques. A frequently adopted approach is based on the use of wavelets to track the local mean magnetic field. Fluctuations within the inertial range at a particular angle of θ_{VB} between the local mean magnetic field and the flow direction can be thus collected to obtain the spectrum in that direction, allowing the investigation of the spectral index at different pitch angles. Horbury et al. (2008), Podesta (2009), Wicks et al. (2010), and Forman et al. (2011) found that the spectral index is close to $-5/3$ when $\theta_{VB} \sim 90°$ and -2 when $\theta_{VB} \sim 0°$, thus providing evidence that critical balance is consistent with solar wind observations. Similar results, consistent with the critical balance predictions, were also obtained by applying multi-point measurement techniques, based on either structure functions (Chen et al. 2011) or the k-filtering method (Roberts et al. 2017), to the four spacecraft Cluster mission data. It is worth mentioning that all of the above results were obtained by investigating the imbalanced Alfvénic fast solar wind.

However, Horbury et al. (2012) noticed that, other than the critically balanced cascade, the observed spectral anisotropy could be possibly caused by the presence of discontinuities in the solar wind, due to, for instance, current sheets (Li et al. 2011). Discontinuities might be accidentally introduced during the mathematical reconstruction of the parallel spectrum, which is indeed not directly obtained in all the methods discussed above, or might be due to the presence of intermittent events in the solar wind. Recently, the influence of intermittency on the spectral anisotropy has been investigated by Wang et al. (2014), who found that its removal from the data leads to shallower parallel spectra. However, the role of intermittency in determining the spectral index is still debated: based on of MHD simulations, Yang et al. (2017) showed that inter-mittency would indeed affect only the perpendicular spectrum and that its removal would not alter the -2 slope of the parallel spectrum. There are very few time instants when the local mean magnetic field is aligned to the wind direction, since the Alfvénic fluctuations, which are transverse to the mean background magnetic field, locally displace it from the direction parallel to the bulk flow. This implies that very long time series are required to build the parallel spectrum (100 days of data points at 1 s resolution in the work by Wicks et al. 2010). However, use of such long data sets implies that the data points used to gather 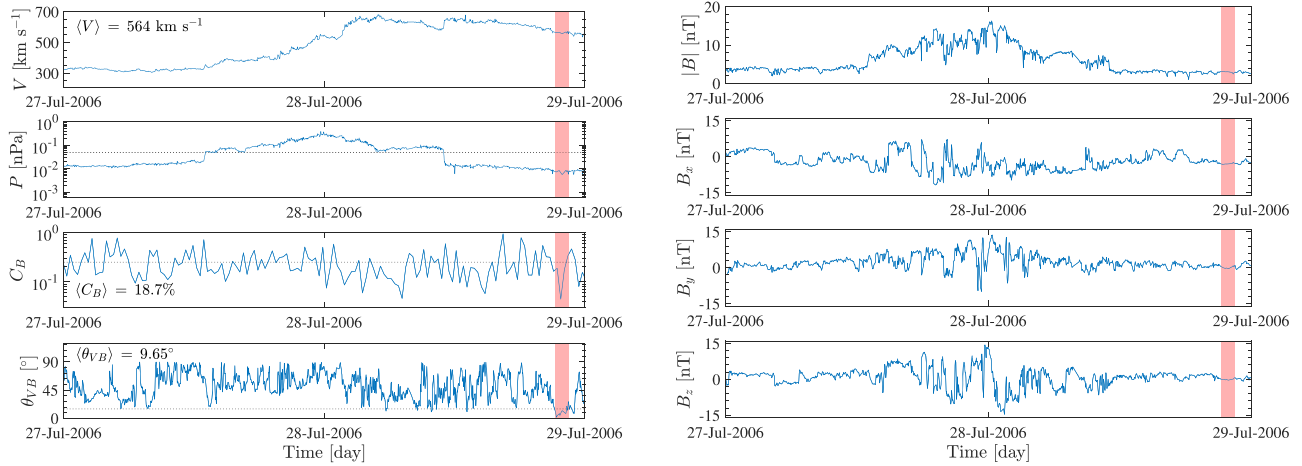the parallel spectrum are randomly distributed along the time period very far from each other (with severe implications on the validity of the solar wind stationarity), thus possibly mimicking a time series of discontinuities.

Wang et al. (2015) first adopted the idea of searching for time intervals where the magnetic field and velocity vectors are aligned, in order not to use the wavelet-based techniques to construct the power spectrum in the parallel direction. They found that the spectral scaling for parallel sampling angles depends on the amplitude of the magnetic fluctuations, which is close to -2 (in agreement with the critical balance conjectures) only for moderate-amplitude fluctuations ($\delta B/B_0 \approx 0.4$). Low-amplitude fluctuations were instead shown to exhibit a spectral scaling close to $-5/3$. However, note that, even if Wang et al. (2015) requires stationarity and randomness for the selected time intervals, they cannot exclude the presence of intermittent events, especially in the moderate-amplitude fluctuation samples, which might play an important role in affecting the spectral scaling of the magnetic fluctuations, as noted by Wang et al. (2014). Furthermore, the estimation of the spectral index might be largely affected also by the poor statistics coming from having considered time intervals that are only six minutes long (as indicated by the wide distribution of the spectral indices shown in Figure 3 of Wang et al. 2015).

To directly probe the solar wind turbulence parallel to the mean background magnetic field and to correctly asses the contribution of intermittency, the following approach is proposed in this paper. First, similarly to Wang et al. (2015), a thorough search of continuous Alfvénic, fast solar wind intervals at least one hour long, mostly populated by $k_\parallel$ fluctuations, is performed in order to avoid possible artifacts derived from using a collection of fragments from distant portions of solar wind. Second, the study of such time periods is performed by the means of the Hilbert spectral analysis (HSA), which is able to remove the possible influence of small-scale noise and large-scale structures from spectral and intermittency properties in the inertial range, thus providing a more accurate estimate of these important characteristics of turbulence. By using these techniques, it is thus possible to measure the spectrum for field-aligned solar wind, exploring the role played by intermittency in the turbulence spectral scaling and eventually providing information on the validity of the critical balance in the solar wind. This is the main aim of the paper, which is organized as follows. A description of the data selection is given in Section 2 and the application of the HSA is provided in Section 3, followed by a discussion of the results and concluding remarks in Section 4.

2. Data Selection

Alfvénic turbulence is often separated in two components, called the slab and 2D (Matthaeus et al. 1990; Zank & Matthaeus 1992; Dasso et al. 2005; Zank et al. 2017), in which fluctuations lie in a plane perpendicular to the global mean background magnetic field, $\boldsymbol{B_0}$. The slab fluctuations propagate along $\boldsymbol{B_0}$, while the 2D advect in planes perpendicular to $\boldsymbol{B_0}$. Thus, the wavevectors of the slab and 2D components are respectively parallel ($\boldsymbol{k_\parallel}$) and perpendicular ($\boldsymbol{k_\perp}$) to the global mean magnetic field. Since critical balance governs the dynamics with respect to the local magnetic field (see Horbury et al. 2012, and references therein), testing its predictions relies on the ability to estimate locally the spectral index of the $k_\parallel$ fluctuations from solar wind measurements. Unfortunately,

Figure 1. Solar wind parameters over the period from 2006 July 27 to 2006 July 29: the bulk speed, total pressure, magnetic compressibility at the scale of 20 minutes, pitch angle, and intensity and components of the magnetic field vector are displayed from top to bottom and from left to right. The shaded area shows 1 of the 17 selected intervals; the averages of solar wind speed, magnetic compressibility, and degree of alignment, relative to this selected data sample. The dotted lines represent the thresholds used in the analysis to select the intervals to be studied.

sampling the solar wind along $\boldsymbol{B_0}$ is rather challenging. Indeed, even when the global mean background magnetic field is aligned to the sampling direction (which coincides with that of the bulk flow), the Alfvénic fluctuations can be large enough to locally lead the solar wind out of alignment. This implies that the locally observed Alfvénic turbulence is predominantly a mix of $k_\perp$ and $k_\parallel$ fluctuations.
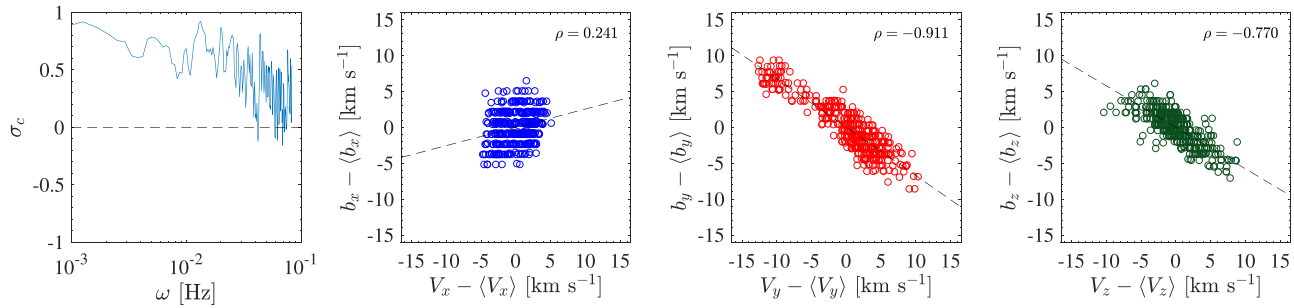
We have undertaken a systematic search of solar wind intervals that robustly provide $k_\parallel$ sampling. We searched 12 yr of solar wind observations, recorded by the *Wind* spacecraft between 2005 and 2016, for intervals satisfying the following requirements: (i) the magnetic field and velocity are aligned within 15° at all scales in the turbulent inertial range, for the whole interval (so that both the local and the global mean magnetic field are *V*-oriented); (ii) each interval has a minimum duration of 1 hr and has no more than 20% of missing data; (iii) intervals only include fast solar wind ($V \geqslant 550\,\mathrm{km\,s^{-1}}$); (iv) intervals are characterized, at the fluid scale of 20 minutes (which is well within the inertial range), by low ($\leqslant 25\%$) magnetic compressibility (defined as the ratio between the variance of the magnetic field intensity fluctuations and the total variance of the fluctuations $C_B = \sigma_{|B|}^2 \big/ \sum_{i=x,y,z} \sigma_{B_i}^2$; Bavassano et al. 1982); and (v) the total pressure of $P = 2nk_\mathrm{B}T + B^2/(8\pi)$ (n and T are the proton number density and temperature, respectively; k_B is the Boltzmann constant; and B is the magnetic field intensity) is smaller than 0.05 nPa to avoid abrupt changes, such as discontinuities or shocks, that can be associated with coronal mass ejections, heliospheric current sheet crossings, or any other magnetic structure. The threshold of 0.05 nPa has been empirically set by performing a statistical analysis of the quasi-steady solar wind over a 12 yr historical data set to localize structures in space plasma characterized by a total pressure higher than the ambient plasma (Telloni et al. 2019). These conditions guarantee that the observed $k_\parallel$ fluctuations belong to undisturbed, Alfvénic, fast solar wind turbulence. As these characteristics are uncommon in the Alfvénic fast solar wind, only 17 intervals were selected out of 12 yr of measurements. The following *Wind* plasma and magnetic field data were considered for the analysis: 92 s resolution space plasma data (including solar wind bulk speed, proton number density and temperature) measured by the Solar Wind Experiment instrument (Ogilvie et al. 1995), and magnetic

field measurements, at a cadence of 92 ms, from the Magnetic Field Investigation magnetometer (Lepping et al. 1995).

Critical balance holds for strong turbulence. For oblique fluctuations, this corresponds to the condition of $(\delta B/B) \cdot (k_\perp/k_\parallel) \sim 1$. Since the energy cascade in the solar wind turbulence is regulated and guided by the large-scale structures, in order to asses whether or not the turbulence is strong, it is necessary to estimate the value of $\delta B/B$ at the scales where the energy is injected—namely at scales larger than a few hours—in the Alfvénic fast wind (e.g., Wicks et al. 2010; Horbury et al. 2012; Chen 2016). The selected 17 field-aligned time intervals are immersed in trailing edges of high-speed streams, where the $\delta B/B$ at injection scales is estimated to be $\gtrsim 0.3$–0.4. Hence, the 17 time intervals studied in this paper are all immersed in strong turbulent flows. The critical balance criterion for strong turbulence is thus satisfied if the sampling direction is such that $k_\parallel/k_\perp = \ell_\perp/\ell_\parallel \sim \delta B/B \gtrsim 0.3$–0.4. It turns out that, in order to ensure a local sampling of parallel fluctuations, the alignment between magnetic and velocity vectors has to be within $\tan^{-1}(\ell_\perp/\ell_\parallel) \sim \tan^{-1}(\delta B/B) \lesssim 17°$–22°. Since, in the present study, magnetic fluctuations are sampled at $\theta_{VB} < 15°$, it can be concluded that $k_\parallel$ fluctuations are indeed locally sampled and that the HSA will provide information on the scaling and intermittency properties of the parallel spectrum in the solar wind turbulence. Within this respect, it is worth recalling that a -2 spectral index consistent with the critical balance predictions was found in strong solar wind turbulence for average pitch angles smaller than 15° (Horbury et al. 2008; Wicks et al. 2010); this represents further indication that requiring that $\theta_{VB} < 15°$ ensures a local parallel sampling of the magnetic fluctuations.

Some relevant parameters relative to 1 of the 17 selected intervals, immersed in a high-speed stream and recorded from 21:13:08 to 22:28:16 UT on 2006 July 28, are shown in the pink shaded area on the right end of both panels of Figure 1, which overall spans from 2006 July 27 to 2006 July 29. From top to bottom and from left to right the figure displays the solar wind speed, the total pressure, the magnetic compressibility evaluated at the fluid scale of 20 minutes, the angle θ_{VB} between the velocity and magnetic field vectors, and the magnetic field intensity and components. The average bulk speed, magnetic compressibility, and pitch angle in the selected

Figure 2. Normalized cross-helicity spectrum, and scatter plots of the velocity and magnetic field component fluctuations (expressed in Alfvén units), during the selected time interval from 21:13:08 to 22:28:16 UT on 2006 July 28, are displayed from left to right. In the scatter plots, the Spearman's rank correlation ρ corresponding to each component (represented by a dashed line) is reported.

time period are $\langle V \rangle = 564\ \mathrm{km\,s^{-1}}$, $\langle C_B \rangle = 18.7\%$, and $\langle \theta_{VB} \rangle = 9°.65$, respectively.

The observation of low magnetic compressibility during the time interval of Figure 1 ($\langle C_B \rangle = 18.7\%$) at fluid scales strongly suggests the Alfvénic nature of the fluctuations. To further confirm this characteristic, we have also evaluated the spectrum of normalized cross-helicity of $\sigma_c = 2\boldsymbol{v} \cdot \boldsymbol{b}/(E_v + E_B)$ ($\boldsymbol{v}$ and $\boldsymbol{b}$ are the velocity and magnetic field vector fluctuations, respectively, and E_v and E_b are the kinetic and magnetic energy, respectively). This is a customary measure of the alignment between magnetic and velocity field fluctuations, so that values of $\sigma_c \simeq \pm 1$ correspond to high levels of Alfvénicity (Belcher & Davis 1971; Tu & Marsch 1995; Bruno & Carbone 2013). As shown in the first panel of Figure 2, $\sigma_c \sim 1$ in the inertial range, clearly confirming that the observed $k_\parallel$ fluctuations are Alfvénic.

A closer look shows that the magnetic–velocity correlations are not present equally in all directions, as indicated by the scatter plots of the fluctuations of the velocity and magnetic field vector components (expressed in Alfvén units, $\boldsymbol{b} = \frac{\boldsymbol{B}}{\sqrt{4\pi\rho}}$, with ρ being the mass density) displayed in the three right panels of Figure 2. Indeed, in the direction parallel to the mean magnetic field (x, corresponding to the heliocentric radial coordinate; the second panel), poor correlations are observed (the Spearman's rank correlation is $\rho = 0.241$), while in the perpendicular plane (y and z directions, third and fourth panels, respectively), magnetic and velocity fluctuations are robustly correlated ($\rho = -0.911$ and $\rho = -0.770$, respectively). This confirms the Alfvénic nature of the $k_\parallel$ fluctuations in the fast wind interval in study.
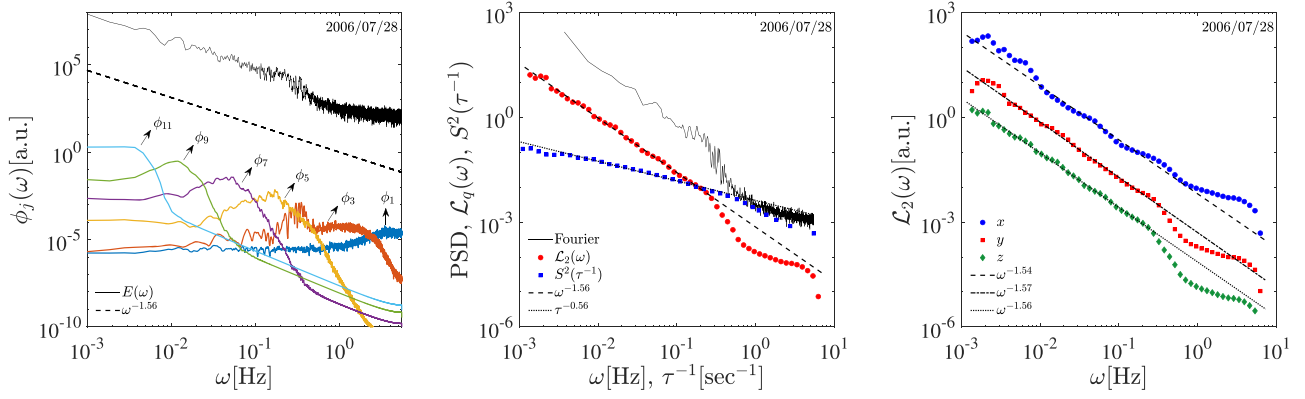
3. Analysis Results

The correct evaluation of the scaling properties of solar wind magnetic fluctuations requires minimizing possible effects of nonstationarity and large-scale ramp-cliff structures embedded in the field. To this aim, an arbitrary-order HSA (Huang et al. 2008, 2011, 2010) has been successfully used recently (Carbone et al. 2016b, 2018; Consolini et al. 2017). HSA relies on an empirical mode decomposition (EMD; Huang et al. 2008), whose basis functions are derived from the signal itself. Using EMD, the effects of spurious harmonics or artifacts near sharp data transitions can be eliminated, improving the performance of the analysis with respect to traditional Fourier or wavelet transforms (Huang et al. 1998; Liu et al. 2012).

In order to evaluate accurately the spectral properties and the degree of intermittency in the magnetic field data (down-sampled to a sampling frequency $Fs = 11$ Hz), an HSA has

been used. The analysis consists of two main steps, which are described briefly as follows.

In the first step, each component of the magnetic field, $\boldsymbol{B}$, is decomposed through the EMD (Huang et al. 1998; Huang & Shen 2005; Jánosi & Müller 2005; McDonald et al. 2007; Vecchio et al. 2014; Carbone et al. 2016b) into a finite number, k, of oscillating basis functions, $\phi_j(t)$, known as intrinsic mode functions (IMFs; Huang et al. 1998; Huang et al. 2008; Flandrin 1999; Cummings et al. 2004; Huang & Shen 2005), so that $B(t) = \sum_{j=1}^{k} \phi_j(t) + r_k(t)$, where $r_k(t)$ is a residual that describes the mean trend (if one exists). EMD acts intrinsically as a dyadic filter bank (Flandrin et al. 2004; Huang & Shen 2005), so that each IMF captures a narrow spectral band in frequency space and can thus be associated to an increasing characteristic timescale, τ (Huang et al. 2008, 2010; Carbone et al. 2016a; Carbone et al. 2018). Examples of the Fourier spectra of some IMF are shown in the left panel of Figure 3, together with the standard Fourier magnetic power spectral density of index $\alpha \approx 1.56 \pm 0.12$. Modes $\phi_j(t)|j > 3$ lie in the inertial range as it emerges from the Fourier spectrum. Their superposition yields a power law of $M(\omega) \equiv \mathrm{Max}[\phi_j(\omega)] \sim \omega^{-\alpha}$, in agreement with the Fourier spectrum (Figure 3, left panel), and is compatible with the standard Kolmogorov prediction (5/3) for fully developed turbulence (Frisch 1995). Note that IMFs $\phi_j(t)|j <= 2$ capture the small-scale dynamics associated with the experimental noise (Cummings et al. 2004; Wu & Huang 2004), highlighted by a clear flattening of the standard Fourier spectrum. On the other hand, larger-scale modes ($\phi_j(t)|j > 11$, not shown) can be associated with large-scale structures, which may contribute to energy injection in the turbulent cascade (Frisch 1995). EMD thus allows us to remove these small-scale and large-scale contributions from the scaling, providing a more accurate evaluation of intermittency (Carbone et al. 2018). Once the IMFs have been obtained, the Hilbert transform of each mode is evaluated as $\phi_j^\star = \frac{p}{\pi} \int_{-\infty}^{+\infty} \phi_j(\tau)(t-\tau)^{-1}d\tau$, where p is the Cauchy principal value and $\phi_j(t)$ is the jth IMF. The combination of $\phi_j(t)$ and $\phi_j^\star(t)$ defines the so-called analytical signal of $\mathcal{Z} = \phi_j + i\phi_j^\star = \mathcal{A}_j(t)e^{i\theta(t)}$, where $\mathcal{A}_j(t)$ is the time-dependent amplitude modulation and $\theta(t)$ is the phase of the mode oscillation (Cohen 1995). The Hilbert spectrum, defined as $H(\omega, t) = \mathcal{A}^2(\omega, t)$ ($\omega = d\theta/dt$ is the instantaneous frequency), provides energy information in the time–frequency domain. A marginal integration of $H(\omega, t)$ provides the Hilbert marginal spectrum of $h(\omega) = T^{-1}\int_0^T H(\omega, t)dt$, defined as the energy density at frequency ω (Huang et al. 1998, 1999). A joint

Figure 3. Left panel: a comparison of Fourier power spectral density, $E(\omega)$ (black line), with the individual Fourier power spectra of six different IMFs $\phi_j(\omega)$ for the interval dated 2006 July 28, as a function of frequency ω (the IMF spectra have been vertically shifted for clarity). The band-like structure of each IMF shows the dyadic nature of the decomposition. The dashed black line indicates the power law of $M(\omega) \sim \omega^{-\alpha}$. Center panel: a comparison of the Fourier power spectrum, $E(\omega)$ (solid line); the Hilbert marginal spectrum, $\mathcal{L}_2(\omega)$ (red circles); and the standard second-order structure function, $S^2(\tau^{-1})$ (blue squares), for the $B_z(t)$ component of the same interval. The three methods show power-law behavior in the inertial range. Power-law fits provide the exponents $\alpha_2^z = 1.56$ (dashed line) and $\zeta(2) = 0.56$. The curves have been vertically shifted for clarity. Right panel: a comparison of the Hilbert marginal spectrum, $\mathcal{L}_2(\omega)$, for the three components of the magnetic field, $\boldsymbol{B}(t)$. A power-law fit provides comparable spectral exponents for all components: $\alpha_2^x \sim 1.54 \pm 0.15$, $\alpha_2^y \sim 1.57 \pm 0.10$, and $\alpha_2^z \sim 1.56 \pm 0.12$.

probability density function, $P(\omega, \mathcal{A})$, can be extracted from the Hilbert spectrum, using the instantaneous frequency, ω_j, and the amplitude, $\mathcal{A}_j$, of the jth IMF. The Hilbert marginal spectrum is then rewritten as $h(\omega) = \int_0^\infty P(\omega, \mathcal{A})\mathcal{A}^2 d\mathcal{A}$, which corresponds to a second-order statistical moment (Huang et al. 2008). The above equation can be finally generalized to the arbitrary order of $q \geqslant 0$ by defining the ω-dependent qth-order statistical moments as

$$\mathcal{L}_q = \int_0^\infty P(\omega, \mathcal{A})\mathcal{A}^q d\mathcal{A} \sim \omega^{-\alpha_q}, \qquad (2)$$

where α_q is the scaling exponents of $\mathcal{L}_q$ usually observed in turbulent flows (Figure 3, right panel). In particular, it can be shown that $h(\omega) \equiv \mathcal{L}_2$ represents the analog of the Fourier spectral energy density (Huang et al. 2008).

In the center panel of Figure 3, the second-order generalized Hilbert spectrum $\mathcal{L}_2(\omega)$ is compared with the standard power spectral density $E(\omega)$ (see left panel of the same figure), showing excellent agreement. A power-law fit $\mathcal{L}_2(\omega) \sim \omega^{-\alpha_2}$ yields $\alpha_2 = 1.56 \pm 0.12$, which is in perfect agreement with the spectral exponent α obtained previously.
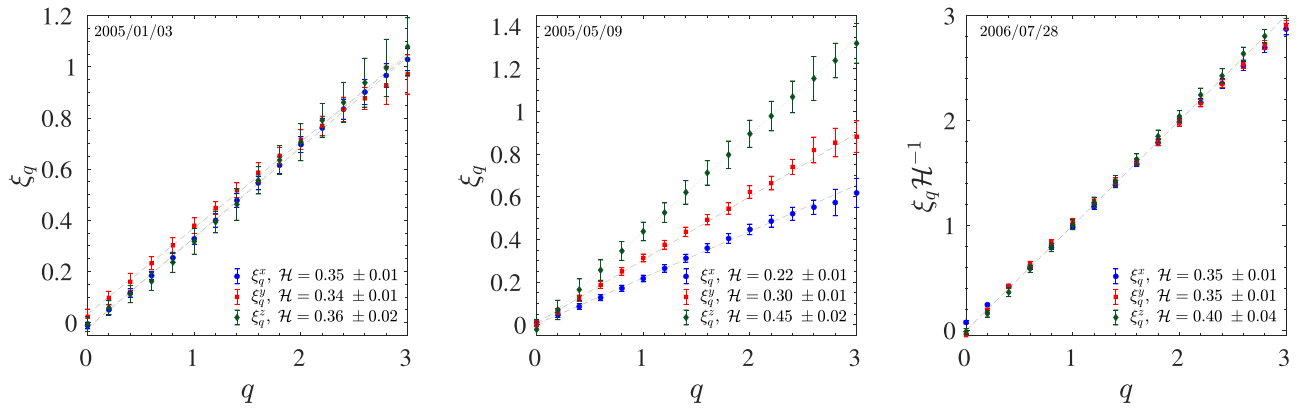
Finally, the Fourier spectral exponent α is known to be linked to the scaling exponent of the second-order structure function (SF) as $S^2(\tau) \equiv \langle |x(t + \tau) - x(t)|^2 \rangle \sim \tau^{\zeta(2)}$ via the relation $E(\omega) \sim \omega^{-\alpha} \to \alpha \equiv \zeta(2) + 1$. A comparison of both the Fourier and Hilbert spectra with the standard second-order structure function, $S^2(\tau)$ (plotted against the inverse scale τ^{-1}), is shown in the center panel of Figure 3, with $\zeta(2) \equiv \alpha - 1 = 0.56$. Similar values were found for all 17 intervals selected for this work, providing the following average and standard deviation (indicated as error) values: $\langle \alpha_2^x \rangle = 1.53 \pm 0.13$, $\langle \alpha_2^y \rangle = 1.71 \pm 0.15$, and $\langle \alpha_2^z \rangle = 1.69 \pm 0.16$. These results robustly indicate that the parallel magnetic spectrum in fast, Alfvénic solar wind is characterized by the typical $-5/3$ spectral index.

In order to evaluate the level of intermittency in the selected samples (Frisch 1995), the previous relations can be extended to any arbitrary-order q to generate the Hilbert analog of the scaling exponents $\zeta(q)$, customarily obtained through the fit of the qth-order structure functions or through extended

self-similarity (Benzi et al. 1993; Arneodo et al. 1996). A set of generalized scaling exponents $\xi(q)$ of the generalized Hilbert spectra (Huang et al. 2010; Carbone et al. 2016a) can thus be introduced as $\xi(q) \equiv \alpha_q - 1$. The dependence of the scaling exponents on the order, and in particular, its deviation from a linear relation $\xi(q) - 1 \propto q\mathcal{H}$ (Huang et al. 2008; Carbone et al. 2018), provides a quantitative estimate of intermittency (Frisch 1995). The scaling exponents $\xi(q)$ obtained from the power-law fit of the generalized Hilbert spectra are shown in Figure 4 for three selected intervals. EMD–HSA comparison shows a nearly linear dependence of the exponents on the order, revealing the absence of intermittency for all three magnetic field components. This was observed consistently for 12 out of the 17 intervals (5 intervals did not show clear power-law spectra), within fitting ranges varying between $\omega \in [10^{-2.5}, 10^{-1}]$ Hz, $\omega \in [10^{-2}, 10^{-1}]$, and $\omega \in [10^{-1.5}, 10^{-0.5}]$. This result exposes the fractal nature of the fluctuations, as opposed to the typical multifractal intermittent fluctuations.

In the classical Kolmogorov theory, in the absence of intermittent corrections the scaling exponents are related to the qth-order moment of the fluctuations via the relation $\zeta(q) = q\mathcal{H}$, where $\mathcal{H}$ is the Hurst number, a parameter that describes the long-term memory (correlated, persistence), or the short-term memory (anticorrelated and anti-persistence) of a process, such that $\alpha_q - 1 = \xi(q) \equiv q\mathcal{H}$.

The first two panels of Figure 4 show the comparison between the scaling exponents $\xi(q)$ obtained from the HSA and the theoretical scaling exponents $q\mathcal{H}$ (Alberti et al. 2019) for two different intervals. In most cases, the three components of the magnetic field have the same Hurst number ($\mathcal{H}^x \approx \mathcal{H}^y \approx \mathcal{H}^z$, see the left panel of Figure 4). In lesser cases, the Hurst numbers are substantially different for the different components, $\mathcal{H}^x \neq \mathcal{H}^y \neq \mathcal{H}^z$ (the center panel of Figure 4), while in other cases, two components are similar and the third is noticeably different (not shown). Finally, in the right panel of Figure 4, the Hurst-normalized scaling exponents $\xi(q)\mathcal{H}^{-1}$ are shown, where $\mathcal{H}$ was obtained though a least square fit of $\xi(q)$ (see the lines in the left and center panels). Despite the small differences among the three components, $\mathcal{H}$ never exceeds the threshold value for uncorrelated processes, $\mathcal{H} < 0.5$. This reveals the presence

Figure 4. Left panel: scaling exponents $\xi(q)$ for the three components of magnetic field $\boldsymbol{B}(t)$ for the interval dated 2005 January 03. Lines represent the theoretical relation of $\xi(q) \equiv q\mathcal{H}$. The maximum order $q_{max} = 3$ was selected in order to accommodate sample size N ($q_{max} \approx \log_{10}[N] - 1$). Center panel: scaling exponents $\xi(q)$ for the three components of the magnetic field for the interval dated 2006 July 28. Right panel: Hurst-normalized scaling exponents $\xi(q)\mathcal{H}^{-1}$ for the sample dated 2006 July 28. The dashed lines represent the bisector of the plane.

of short range correlations (anti-persistence), characterized by the average and standard deviation of $\langle\mathcal{H}^x\rangle \approx 0.27 \pm 0.07$, $\langle\mathcal{H}^y\rangle \approx 0.34 \pm 0.08$, $\langle\mathcal{H}^z\rangle \approx 0.34 \pm 0.09$, which are in perfect agreement with other estimates (Consolini et al. 2017).

Within these values, the second-order moment (the Fourier power spectrum) is always compatible with the observed power-law scaling of $\mathcal{L}_2 \sim \omega^{-\alpha_2}$, with $\alpha_2 \equiv 2\mathcal{H} + 1 \approx 1.66$, which is characteristic of the classical Kolmogorov spectrum.

4. Discussion and Conclusions

This paper provides observational evidence that the $k_\parallel^{-5/3}$ magnetic power spectrum is observed persistently in the strong Alfvénic fast solar wind turbulence in the direction parallel to the local mean magnetic field, thus arising questions regarding the validity of the critical balance theory in the solar wind turbulence. These results are consistent with those in Wang et al. (2015), who used a database of time intervals six minutes long that share similar properties with the solar wind samples analyzed in this work (i.e., a small relative amplitude of $\delta B/B \sim 0.1$ around 10^{-3} Hz), finding a $-5/3$ slope in field-aligned configurations. The HSA applied in this study to the selected 17 time intervals furthermore allows us to show, for the first time, that the fast, Alfvénic solar wind is weakly (or even not at all) intermittent along the mean background magnetic field $\boldsymbol{B_0}$. This suggests a possible relation between the presence of intermittency and the energy spectra scaling, as proposed by Wang et al. (2014). In fact, these authors found that when intermittency is removed from data, the spectral scaling is close to $-5/3$ regardless of the angle between the local mean magnetic field and the flow direction.

Similar results were also observed for a single polar solar wind interval, satisfying the search criteria described above, as observed by Ulysses during the period analyzed by Wicks et al. (2010). It can be concluded that Kolmogorov-like scaling ($E(k_\parallel) \propto k_\parallel^{-5/3}$) and nearly self-similar scaling (no or weak intermittency) represent robust characteristics of the Alfvénic solar wind with $k_\parallel$ magnetic fluctuations—namely the slab component of solar wind turbulence.

A possible explanation for the observed characteristics may be given in terms of the stochastic nature of the parallel magnetic fluctuations. In fact, any self-similar stochastic process (i.e., fractional Brownian motion), characterized by Hurst number $\mathcal{H} \approx 1/3$, will result in a power spectral index

close to the Kolmogorov-like scaling. Such fluctuations are mostly short-term correlated, resulting in the absence of intermittency. In this sense, intermittency is usually considered as a fundamental ingredient of the nonlinear turbulent cascade in the fluid turbulence community (Frisch 1995), as well as in the reduced MHD (Mallet et al. 2016). In this interpretation, the parallel magnetic fluctuations may not be the result of a nonlinear cascade, but rather a superposition of uncorrelated Alfvénic fluctuations. The weak intermittency observed in some of the intervals could be simply attributed to a local time variation of the stochastic properties of the fluctuations represented by $\mathcal{H}$ (Ayache & Véhel 1999; Ayache & Vehel 2000; Stoev & Taqqu 2006; Huang & Schmitt 2016). In a simplified view, the absence of intermittency can be explained by supposing that the inner heliosphere is permeated by filamentary structures, such as magnetic flux tubes, separated by tangential discontinuities (Bruno et al. 2001). These interplanetary "spaghetti-like" structures, characterized by different plasma parameter values and by a different magnetic field intensity and orientation, would contain imbedded pure Alfvénic local fluctuations. In this scenario, a spacecraft moving across adjacent flux tubes would sample an intermittent signal. On the other hand, since the fluctuations within each flux tube are purely Alfvénic, a spacecraft sampling the solar wind along the mean local magnetic field (thus measuring only $k_\parallel$ fluctuations) would detect non-intermittent fluctuations, as observed in the intervals studied in this paper.

However, recent theoretical results offer a possible alternative scenario in which the turbulent cascade (and a $k_\parallel^{-5/3}$ magnetic spectrum) could be activated even for reduced or absent nonlinear interactions among oppositely directed Alfvén modes, thus supporting the results obtained in this paper, which indicate that quasi uni-directional propagating Alfvén waves ($\sigma_c \approx \pm 1$) may produce a Kolmogorov-like turbulent spectrum. The origin of this spectrum may be explained in the framework of the nearly incompressible superposition model by Zank et al. (2017), which describes the turbulence as a majority (quasi-)2D component and a minority slab component. The field-aligned samples of solar wind analyzed in the present work ensure to pick out only the $k_\parallel$ Alfvén fluctuations but not the advected 2D component (non-propagating $k_\perp$ fluctuations lying in the plane orthogonal to the magnetic field),

which are, however, still present. As shown in Zank et al. (2017), the quasi-2D modes couple in a "passive-scalar" sense to the slab fluctuations at the nonlinear timescale. This coupling, which occurs for any σ_c, even in the presence of uni-directional Alfvén wave propagation (as also shown in Adhikari et al. 2019, where the slab turbulence does not turn off when $\sigma_c = \pm 1$), naturally leads to a $k_{\parallel}^{-5/3}$ slab spectrum. However, the Zank et al. (2017) model does not include predictions about intermittency. The observed absence of intermittency suggests the need for an extension of the model for a more conclusive comparison. This is left for a future dedicated work.

The results presented in this work will be relevant to the *Parker Solar Probe* and *Solar Orbiter* missions, whose orbital characteristics are likely to sample solar wind intervals with the required characteristics to confirm our observations and additionally study the radial evolution of such turbulence.

ORCID iDs

Daniele Telloni ⬤ https://orcid.org/0000-0002-6710-8142
Francesco Carbone ⬤ https://orcid.org/0000-0002-3559-5273
Roberto Bruno ⬤ https://orcid.org/0000-0002-2152-0115
Luca Sorriso-Valvo ⬤ https://orcid.org/0000-0002-5981-7758
Gary P. Zank ⬤ https://orcid.org/0000-0002-4642-6192
Laxman Adhikari ⬤ https://orcid.org/0000-0003-1549-5256
Peter Hunana ⬤ https://orcid.org/0000-0002-9860-9759

References

Adhikari, L., Zank, G. P., Telloni, D., et al. 2017, ApJ, 851, 117
Adhikari, L., Zank, G. P., & Zhao, L.-L. 2019, ApJ, 876, 26
Alberti, T., Consolini, G., Carbone, V., et al. 2019, Entrp, 21, 320
Arneodo, A., Baudet, C., Belin, F., et al. 1996, EL, 34, 411
Ayache, A., & Véhel, J. L. 1999, in Fractals: Theory and Applications in Engineering, ed. M. Dekking et al. (London: Springer), 17
Ayache, A., & Vehel, J. L. 2000, in Statistical Inference for Stochastic Processes, ed. Y. A. Kutoyants & S. Hörmann, Vol. 3 (London: Springer), 7
Bavassano, B., Dobrowolny, M., Fanfoni, G., Mariani, F., & Ness, N. F. 1982, SoPh, 78, 373
Belcher, J. W., & Davis, L., Jr. 1971, JGR, 76, 3534
Benzi, R., Ciliberto, S., Tripiccione, R., et al. 1993, PhRvE, 48, R29
Boldyrev, S. 2006, PhRvL, 96, 115002
Bruno, R., & Carbone, V. 2013, LRSP, 10, 2
Bruno, R., Carbone, V., Veltri, P., Pietropaolo, E., & Bavassano, B. 2001, P&SS, 49, 1201

Carbone, F., Gencarelli, C. N., & Hedgecock, I. M. 2016a, PhRvE, 94, 063101
Carbone, F., Landis, M. S., Gencarelli, C. N., et al. 2016b, GeoRL, 43, 7751
Carbone, F., Sorriso-Valvo, L., Alberti, T., et al. 2018, ApJ, 859, 27
Chen, C. H. K. 2016, JPlPh, 82, 535820602
Chen, C. H. K., Mallet, A., Yousef, T. A., Schekochihin, A. A., & Horbury, T. S. 2011, MNRAS, 415, 3219
Cohen, L. 1995, Time-frequency Analysis (Englewood Cliffs, NJ: Prentice Hall PTR)
Consolini, G., Alberti, T., Yordanova, E., Marcucci, M. F., & Echim, M. 2017, JPhCS, 900, 012003
Cummings, D. A., Irizarry, R. A., Huang, N. E., et al. 2004, Natur, 427, 344
Dasso, S., Milano, L. J., Matthaeus, W. H., & Smith, C. W. 2005, ApJ, 635, L181
Flandrin, P. 1999, Time-Frequency/Time-Scale Analysis, Wavelet Analysis and Its Applications 10 (1st ed.; New York: Academic)
Flandrin, P., Rilling, G., & Goncalves, P. 2004, ISPL, 11, 112
Forman, M. A., Wicks, R. T., & Horbury, T. S. 2011, ApJ, 733, 76
Frisch, U. (ed.) 1995, Turbulence: The Legacy of A.N. Kolmogorov (Cambridge: Cambridge Univ. Press)
Goldreich, P., & Sridhar, S. 1995, ApJ, 438, 763
Horbury, T., Wicks, R., & Chen, C. 2012, SSRv, 172, 325
Horbury, T. S., Forman, M., & Oughton, S. 2008, PhRvL, 101, 175005
Huang, N. E., & Shen, S. S. P. (ed.) 2005, The Hilbert-Huang Transform and Its Applications (Singapore: World Scientific)
Huang, N. E., Shen, Z., & Long, S. R. 1999, AnRFM, 31, 417
Huang, N. E., Shen, Z., Long, S. R., et al. 1998, RSPSA, 454, 903
Huang, Y., & Schmitt, F. G. 2016, Stochastic Analysis of Scaling Time Series: from Turbulence Theory to Applications (Cambridge: Cambridge Univ. Press)
Huang, Y. X., Schmitt, F. G., Hermand, J.-P., et al. 2011, PhRvE, 84, 016208
Huang, Y. X., Schmitt, F. G., Lu, Z. M., et al. 2010, PhRvE, 82, 026319
Huang, Y. X., Schmitt, F. G., Lu, Z. M., & Liu, Y. L. 2008, EL, 84, 40010
Iroshnikov, P. S. 1964, SvA, 7, 566
Jánosi, I. M., & Müller, R. 2005, PhRvE, 71, 056126
Kraichnan, R. H. 1965, PhFl, 8, 1385
Lepping, R. P., Acúna, M. H., Burlaga, L. F., et al. 1995, SSRv, 71, 207
Li, G., Miao, B., Hu, Q., & Qin, G. 2011, PhRvL, 106, 125001
Lithwick, Y., Goldreich, P., & Sridhar, S. 2007, ApJ, 655, 269
Liu, Q., Fujita, T., Watanabe, M., & Mitani, Y. 2012, in IFAC Proc. Volumes 45, VIII Power Plant and Power System Control Symposium (New York: Elsevier), 144
Mallet, A., Schekochihin, A. A., Chandran, B. D. G., et al. 2016, MNRAS, 459, 2130
Matthaeus, W. H., Goldstein, M. L., & Roberts, D. A. 1990, JGR, 95, 20673
McDonald, A. J., Baumgaertner, A. J. G., Fraser, G. J., George, S. E., & Marsh, S. 2007, AnGeo, 25, 375
Montgomery, D., & Turner, L. 1981, PhFl, 24, 825
Ogilvie, K., Chornay, D., Fritzenreiter, R., et al. 1995, SSRv, 71, 55
Podesta, J. J. 2009, ApJ, 698, 986
Roberts, O. W., Narita, Y., & Escoubet, C. P. 2017, ApJ, 851, L11
Shebalin, J. V., Matthaeus, W. H., & Montgomery, D. 1983, JPlPh, 29, 525
Stoev, S. A., & Taqqu, M. S. 2006, Stochastic Processes Appl., 116, 200
Telloni, D., Antonucci, E., Bemporad, A., et al. 2019, ApJ, 885, 120
Tu, C., & Marsch, E. 1995, SSRv, 73, 1
Vecchio, A., Anzidei, M., & Carbone, V. 2014, JGeo, 79, 39
Wang, X., Tu, C., He, J., Marsch, E., & Wang, L. 2014, ApJ, 783, L9
Wang, X., Tu, C., He, J., et al. 2015, ApJ, 810, L21
Wicks, R. T., Horbury, T. S., Chen, C. H. K., & Schekochihin, A. A. 2010, MNRAS Letters, 407, L31
Wu, Z., & Huang, N. E. 2004, RSPSA, 460, 1597
Yang, L., He, J., Tu, C., et al. 2017, ApJ, 846, 49
Zank, G. P., Adhikari, L., Hunana, P., et al. 2017, ApJ, 835, 147
Zank, G. P., & Matthaeus, W. 1992, JGR, 97, 17189